ANALYSIS OF TERRAIN MODELLING METHODS IN THE COASTAL ZONE

Oktawia Lewicka

Department of Geodesy and Oceanography, Gdynia Maritime University, Gdynia, Poland and Marine Technology Ltd., Gdynia, Poland

E-mail of corresponding author: o.lewicka@wn.umg.edu.pl, o.lewicka@marinetechnology.pl

Oktawia Lewicka 0000-0002-0382-2793

Resume

Geospatial data are increasingly used to model the terrain in the coastal zone, in particular in shallow waterbodies (with a depth of up to 1 m). In order to generate a terrain relief, it is important to choose a method for its modelling that will allow it to be accurately projected. Therefore, the aim of this publication is to analyze the terrain modelling methods in the coastal zone. For the purposes of the research, five most popular methods for terrain modelling were described: Inverse Distance Weighted (IDW), Modified Shepard's Method (MSM), Natural Neighbor Interpolation (NNI), kriging and spline. Each of the methods has been described in a uniform way in terms of: the essence of its operation, mathematical expression and application examples. The advantages and disadvantages of each of the methods for terrain modelling are also discussed. It should be stated that the choice of the method for the terrain modelling of a shallow waterbody is not unambiguous, as it depends on the type of data recorded during bathymetric and photogrammetric measurements.

Article info

Received 29 December 2022
Accepted 28 February 2023
Online 6 April 2023

Keywords:

terrain modelling
coastal zone
inverse distance weighted (IDW)
modified shepard's method (MSM)
natural neighbor interpolation (NNI)
kriging
spline

Available online: https://doi.org/10.26552/com.C.2023.041

ISSN 1335-4205 (print version)
ISSN 2585-7878 (online version)

1 Introduction

Geodetic and hydrographic measurements are increasingly carried out by Unmanned Aerial Vehicles (UAV), Unmanned Surface Vehicles (USV) or Terrestrial Laser Scanners (TLS) [1-3]. The use of these modern methods in coastal zone measurements enables the acquisition of high-quality bathymetric data. However, these data do not cover the total area of the seabed [4]. For this reason, data interpolation methods, which create Digital Terrestrial Models (DTM), are used [5]. Hence, it is important to know that the creating of a DTM is a multi-stage process (Figure 1).

Creation of a DTM requires prior data collection. In addition to the above-mentioned measurement equipment, the following measurement methods are used to obtain the land surface geospatial data:

- Direct field measurements - they consist of the position survey or height of objects in the field. Currently, modern electronic total stations and Global Positioning System (GPS) receivers are used for direct measurements. The data obtained by the direct method are characterized by high accuracy. However, a direct field survey is time-consuming and thus provides small amount of data [6-8];
- Photogrammetric measurements - a measurement method consisting in recreating a ray going from the camera lens to the select point using a camera. Surveys provide information about the shape of the object and its position in relation to other objects in space [9]. UAVs equipped with cameras are increasingly used to take photogrammetric images. Moreover, photogrammetric data can be derived from aerial or satellite images [10-11];
- Bathymetric measurements - they consist of obtaining the processed data on the depth distribution in a waterbody. Bathymetric measurements are usually performed using a Single Beam Echo Sounder (SBES) or a MultiBeam Echo Sounder (MBES). A limitation of the measurement method using a SBES is the lack of depth data between profiles [12-13];
- Map vectorization - consists of converting the raster data into vector data. Map vectorization can

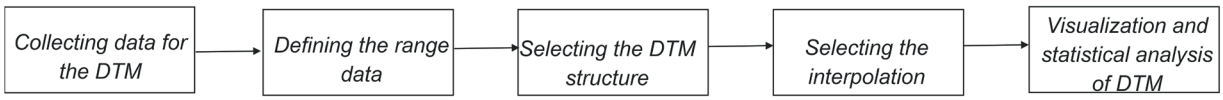

Figure 1 *A diagram showing the stages in creating a DTM*

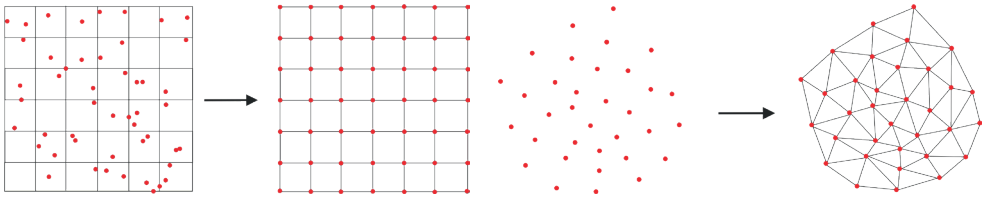

(a) *(b)*

Figure 2 *A diagram showing the structure of a GRID (**a**) and a TIN (**b**)*

be performed using the Geographic Information System (GIS) software, e.g. ArcGIS, GeoMedia or QGIS. The data acquired by this method are affected by errors associated with coordinate transformation [14-15];

- Laser scanning measurements - surveys in which the system measures the distance and the angle between the instrument and the surface being measured [16]. Laser scanning surveys can be performed using either Airborne Lidar Bathymetry (ALB) or Terrestrial Laser Scanning (TLS). Data obtained from the laser scanning are characterized by high accuracy [17-18];
- Interferometric Synthetic Aperture Radar (InSAR) - a method that measures the spatial extent and magnitude of surface deformation. It is a remote sensing method that uses the phase difference between the two complex radar SAR observations of the same area, taken from slightly different sensor positions [19-20].

The next stage in creating the model is to define the data range. An important aspect of data preparation is their density and distribution. Therefore, it is to be expected that data distributed unevenly due to interpolation will create a DTM that will not faithfully reproduce the surface.

Subsequently, the method of DTM representation, i.e. the structure of the model, is determined. The following ways of representing a DTM are distinguished [21]:

- A regular square grid (GRID) (Figure 2a) - a form of DTM representation, in the shape of a squares grid that covers an area evenly. The GRID models are created through interpolation, i.e. estimating an unknown value based on known values and specific interpolation methods. Next, the GRID nodes are created, which form a structure of regular rectangles (usually squares) with a determined resolution;
- Triangulated Irregular Network (TIN) (Figure 2b) - a form of DTM representation, in the shape of an irregular network of triangles. The TIN structure is formed by adjacent triangles whose vertices are located at the real measurement points. These points should be relatively evenly distributed for a network comprising triangles with similar shapes to be created. Where a surface is covered with measurement points unevenly (in a dispersed or linear manner), elongated triangles with no regular shapes will be formed.

After choosing the DTM representation structure, the data interpolation method needs to be selected, which is the most important stage in creating a digital terrain model. As regards the interpolation methods, the two main groups of spatial models can be distinguished:

- Deterministic models - values are determined based on the distance or area function. The deterministic models include, among others the Inverse Distance Weighted (IDW), polynomial and spline [22];
- Statistical models - values are determined based on the probability theory. The statistical methods include kriging and regression models.

The final stage of work is the visualization of the DTM. Additionally, it is recommended that an assessment of accuracy of the generated models be conducted using typical accuracy measures [23]: Root Mean Square Error (RMSE) [24], Mean Absolute Error (MAE) [25] and the coefficient of determination (R^2).

The terrain modelling methods have found applications in many scientific fields. In geology, the interpolation methods are used, e.g. to model geological [26] and geomorphological processes [1], as well as geological structures [27]. It is also worth noting the fact that the interpolation methods can be used to create Electronic Navigational Charts (ENC), which contain a detailed description of hydrographic structures and waterbody depths. In addition, they are the basic source of information in marine navigation [28].

However, a DTM has a particular application in the coastal zone. A model generated in this area enables the study of oceanographic phenomena and processes, as well as modelling of coastline changes. Nevertheless, it poses a research problem of selecting the most accurate method for modelling the surface in the coastal zone.

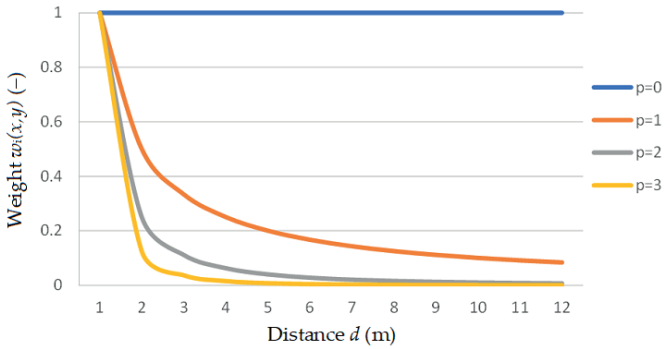

Figure 3 *A diagram showing the relationship between the weight $w_i(x,y)$ with the exponent p and the distance d*

Therefore, it was decided to characterize popular data interpolation methods.

The paper consists of three sections. The first section (Introduction) provides a detailed description of the stages in creating a DTM. The second section (Interpolation methods) presents five most popular methods for terrain modelling: IDW, Modified Shepard's Method (MSM), Natural Neighbor Interpolation (NNI), kriging and spline. Each of the methods has been described in a uniform way in terms of: the essence of its operation, mathematical expression and application examples. The publication concludes with Conclusions, which sum up the methods described.

2 Interpolation methods

2.1 IDW

The most commonly used deterministic model in spatial interpolation is the IDW method, which involves the estimation of the value being interpolated by calculating a weighted average from the values located at a specific distance from the point being interpolated [29].

The height value of the interpolated point by the IDW method can be calculated using the following formula [30]:

$$z_{IDW}(x,y) = \frac{\sum_{i}^{n} w_i(x,y) \cdot z_i}{\sum_{i}^{n} w_i(x,y)}, \tag{1}$$

where:
$z_{IDW}(x,y)$ - height value of the interpolated (unknown) point by the IDW method (m);
x, y - easting and northing of the interpolated (unknown) point (m);
n - number of interpolating (known) points (-);
i - numbering representing successive interpolating (known) points (-);
$w_i\ (x,y)$ - weight value of the i-th point in the IDW method (-);
z_i - height value of the i-th point (m).

However, the weight values are inversely proportional to the distance between the interpolated (unknown) point and the interpolating (known) point [31]:

$$w_i(x,y) = \frac{1}{[d_i(x,y)]^p}, \tag{2}$$

where:
p - exponent (-);
$d_i(x,y)$ - actual distance between the interpolated (unknown) point and the i-th point, defined as follows (m):

$$d_i(x,y) = \sqrt{(\Delta x_i)^2 + (\Delta y_i)^2} = \sqrt{(x - x_i)^2 + (y - y_i)^2} \tag{3}$$

where:
x_i, y_i - easting and northing of the i-th point (m).

A factor affecting the shape of the surface being modelled is dependent on the value of the exponent p. Application of the exponent p as the weight function is referred to in the literature as the Inverse Distance to a Power (IDP) method [32-33]. Usually, a basic exponent value of p = 2 or p = 3 is applied. However, application of these exponents does not always result in representation of the actual surface. Based on the weight function, it can be concluded that it decreases with an increase in distance. An increased exponent results in the weight decreasing its value (Figure 3) [34].

Another parameter that has an effect on the surface mapping is the smoothing parameter. The modified IDW method, to include the smoothing parameter, is as follows [35]:

$$z'_{IDW}(x,y) = \frac{\sum_{i}^{n} \frac{1}{[d_i(x,y) + \sigma]^p} \cdot z_i}{\sum_{i}^{n} \frac{1}{[d_i(x,y) + \sigma]^p}}, \tag{4}$$

where:
σ - smoothing parameter (m).

A high value of the smoothing parameter σ results in the target interpolating value having less influence on the interpolated value. Moreover, in order to smooth

the modelled surface, independent smoothing methods are used [36].

The next additional parameter in the modified IDW method is the effective distance. It is used when the phenomenon of anisotropy is considered in the data interpolation procedure. This phenomenon involves a change in properties of an object depending on the direction of observation of a particular feature. This means that values of the interpolating data change depending on the direction under consideration [37].

In the modified IDW method, which considers the phenomenon of anisotropy, the actual distance is replaced by the effective distance [38]. The modified IDW method can be written using Equation (4). However, the distance between the measurement point and the interpolated point has the following form [35, 39]:

$$d_i'(x,y) = \sqrt{\begin{matrix} A_{xx}\cdot(\Delta x_1)^2 + A_{xy}\cdot\Delta x_i\cdot\Delta y_i + \\ + A_{yy}\cdot(\Delta y_i)^2 \end{matrix}}, \tag{5}$$

where:
$d_i'(x,y)$ - effective distance between the interpolated (unknown) point and the i-th point (m).

The unknown parameters in the formula for the effective distance are determined as follows [35, 39]:

$$A_{xx} = \sin^2(\theta) + \frac{\cos^2(\theta)}{\rho^2}, \tag{6}$$

$$A_{xy} = 2\cdot\left[\frac{\sin(\theta)\cdot\cos(\theta)}{\rho^2} - \sin(\theta)\cdot\cos(\theta)\right], \tag{7}$$

$$A_{yy} = \frac{\sin^2(\theta)}{\rho} + \cos^2(\theta), \tag{8}$$

where:
θ - anisotropy angle (°);
ρ - anisotropy ratio (-).

It should be noted that an anisotropy ratio value smaller than 2 has no significant impact on interpolation, while a ratio value greater than 4 has such an impact.

The IDW method, along with its numerous modifications, is the most commonly used method for modelling phenomena and surfaces. It has found application in many areas of scientific research, particularly in the coastal zone modelling. An example is a study presented in [31], which created a DTM of the coastal zone by the IDW method. Moreover, the generated models enabled a geospatial analysis of the tombolo phenomenon in a waterbody adjacent to the beach in the city of Sopot. It should be noted that the IDW method was applied without using additional parameters, such as the anisotropy, exponent and smoothing. On the other hand, the depth data were derived from the SBES and the data from ENC cells were used.

Another example of the IDW application is described in a publication by Maleika [36]. The method was tested on data from an MBES, and its parameters were modified in terms of accuracy. A research problem in this study was the density of the data being entered into the IDW method, as having too many measurement points during the interpolation increases the model error and significantly increases the computation time. Therefore, based on different modifications of the IDW method, it was determined that the best results were obtained for 5-8 measurement points located within a radius of 0.6 m. Based on a study by Maleika [36], it should be concluded that the IDW method enables the modification of parameters, which translates into the method fitting to obtain the best results. The next example of the IDW application is presented in an article by Lubczonek et al. [1]. It is noteworthy that the IDW method was applied to data derived from an UAV and an USV. The integration of the data derived from these two systems enabled creation of a model of a bathymetric surface extending to the coastline.

2.2 MSM

The MSM method is another modification of the IDW method. It appears in the literature as an independent numerical method, which is why it was decided to characterize it in a separate subsection. The method was developed to reduce the expressive local values, which result in the so-called bull's-eye or the butterfly shape. The MSM method was developed by Shepard in 1968 [40] and implemented in studies by Franke and Nielson [41], Renka [42] and Basso et al. [43].

The MSM function has the following equation [42-44]:

$$z_{MSM}(x,y) = \frac{\sum_i^n w_i'(x,y)\cdot Q_i(x,y)}{\sum_i^n w_i'(x,y)}, \tag{9}$$

where:
$z_{MSM}(x,y)$ - height value of the interpolated point by the MSM method (m);
$w_i'(x,y)$ - weight value of the i-th point in the MSM method (-);
$Q_i(x,y)$ - bivariate quadratic function of the i-th point (-).

The bivariate quadratic function is the second-degree polynomial with one or more variables, which is calculated by the least squares method for the selected reference points [45]:

$$\begin{matrix} Q_i(x,y) = a\cdot(x-x_i) + b\cdot(y-y_i) + c\cdot(x-x_i)^2 + \\ + d\cdot(y-y_i)^2 + e\cdot(x-x_i)\cdot(y-y_i) + f, \end{matrix} \tag{10}$$

where:
a, b, c, d, e - numerical coefficients (-);
f - constant of the quadratic function (-).

The polynomial function $Q_i(x,y)$ describes a quadratic surface [46], which is a conic section. Depending on the coefficients a, b, c, d, e and f, the conic section is a circle, ellipse, hyperbola, parabola, point or two straight lines.

It should be noted that the second-degree polynomial $Q_i(x,y)$ is solved by the least squares method [47]. The use of this method allows the data to be fitted to the conic section. The least squares method is used to determine a conic section for which the sum of squared errors will be the smallest, and thus the sum of distances of all points from the conic section will be minimum.

The weight function, as suggested by Franke and Nielson [41], has the following form:

$$w_i'(x,y) = \left[\frac{(R_w - d_i(x,y))_+}{R_w \cdot d_i(x,y)}\right]^2 \text{ for } (R_w - d_i(x,y))_+ = \begin{cases} R_w - d_i(x,y) & if \quad d_i(x,y) < R_w \\ 0 & if \quad d_i(x,y) \geq R_w \end{cases}, \tag{11}$$

where:
R_w - radius of influence around the i-th point (m).

In the modified IDW method with the radius parameter, in the weight function [48], the radius value determines the decrease in the weight with an increasing radius R_w. The radius R_w, exactly like the exponent used in the IDW method, enables the smoothing of the modelled surface. Moreover, an accurate representation of the surface is obtained for the coefficient R_w equal to the distance from the furthest interpolating point [34].

Derivation of the second-degree equation to the IDW results in an unrealistic landform on the edges. This is due to the merging of extreme points on the interpolated area edges that does not refer to the overall variability trend. Consequently, the MSM method smooths surfaces, thus eliminating outliers.

The MSM method was compared to the IDW method in [44]. The methods were applied to a small data set. The input data for the models included the permeability, porosity and thickness of the Neogene hydrocarbon sandstone reservoirs in northern Croatia. The cross-validation results proved that the MSM method could be recommended for geological mapping of the Neogene deposits. Moreover, the MSM method eliminated all unwanted geological features in the model.

2.3 NNI

The simplest approach to interpolation was applied in the NNI method. This method was introduced for the first time by Sibson [49] as a weighted average weighted interpolation method. Additionally, research concerning the structure and properties of the method are described in studies by Farin [50] and Piper [51].

The height value of the interpolated point by the NNI method can be calculated using the following formula [52]:

$$z_{NNI}(x,y) = \sum_j^m w_j(x,y) \cdot z_j\,, \tag{12}$$

where:
$z_{NNI}(x,y)$ - height value of the interpolated (unknown) point by the NNI method (m);
m - number of neighboring points (-);
j - numbering representing successive neighboring points (-);
$w_j(x,y)$ - weight value of the j-th point in the NNI method (-);
z_j - height value of the j-th point (m).

The weight value according to Sibson [49, 53] is the quotient of the stolen area of the j-th Voronoi cell [54] for the whole area of the new Voronoi cell [55]:

$$w_j(x,y) = \frac{S_j}{S}\,, \tag{13}$$

where:
S_j - stolen area of the j-th Voronoi cell (m²);
S - whole area of the new Voronoi cell (m²).

Using the previous Equations (12) and (13), the following equation was obtained:

$$z_{NNI}(x,y) = \sum_j^m \frac{S_j}{S} \cdot z_j\,. \tag{14}$$

It should be noted that the Voronoi diagram method [56] consists in a creation of irregular polygons based on the analyzed points and then entering of the corresponding point value into each polygon. In the literature, this method is also referred to as Thiessen diagrams or polygons. This is due to the fact that the article published in 1911 by an American meteorologist Alfred H. Thiessen proposed a method for determining the average amount of precipitation over the study area [57-58]. This method used the same polygons for the calculations as Voronoi diagram method.

The procedure for constructing the Voronoi diagram consists of the following stages (Figure 4) [59]:

A. Selection of measurement points for the construction the Voronoi diagram;

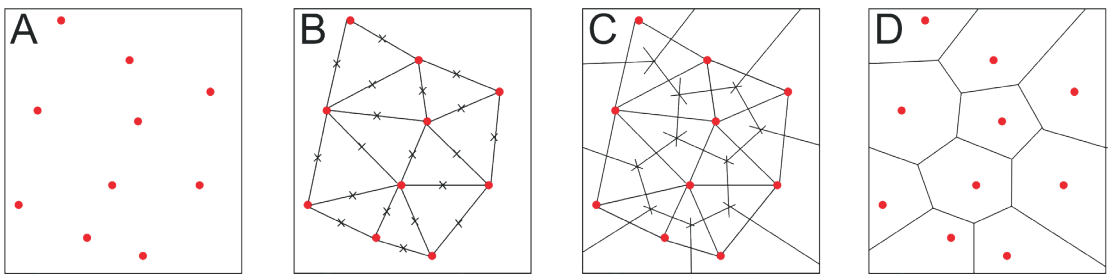

Figure 4 *The process of creating the Voronoi diagram [59]*

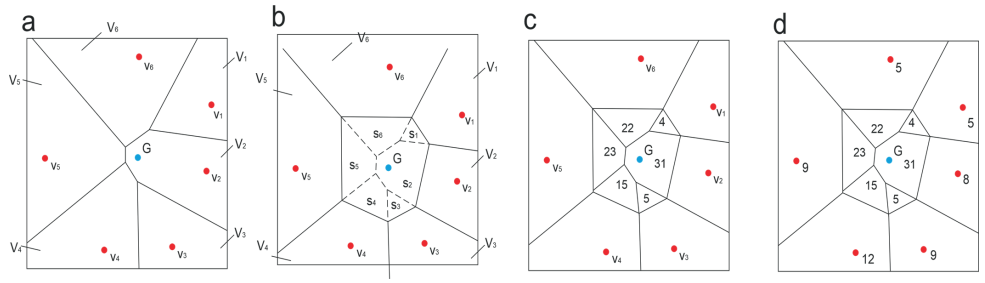

Figure 5 *A diagram showing the constructions and calculations for the NNI method based on the example from [60]*

B. Determination of sections between the most closely located points;
C. Drawing perpendicular bisectors for each section;
D. Connecting each of the points where the three bisectors intersect.

On the other hand, the diagram of the interpolation procedure by the NNI method is as follows (Figure 5):

a. Creation of the Voronoi diagram for all the measurement points;
b. Creation of the Voronoi diagram for the point G being interpolated;
c. Determination of the proportion of particular polygons S_1, S_2, S_3, S_4, S_5, S_6 for the polygon G;
d. Calculation of the height value for the point G by the NNI method using Equation (13).

Based on the presented diagrams and equations, it can be concluded that this is a not very complicated method, which means that it can be easily implemented. Moreover, the method is mainly based on forming of a network of triangles by the Voronoi method, which is created locally in relation to the interpolating point. Unlike the other methods, the NNI method has no global data structure and only uses the data which are adjacent to the interpolated value. Therefore, the NNI method can be used for unevenly distributed data. This is confirmed by research conducted in [61]. The NNI method has proven to be more accurate than the IDW, kriging or spline methods.

2.4 Kriging

Geostatistical methods are based on finding a function which determines the similarity of points based on the mutual relationships occurring between them. One such method is kriging. This method was originally developed by Krige [62] for the purposes of a Master's degree thesis, in which he tried to estimate the most likely distribution of gold based on samples from a few boreholes. On the other hand, the theoretical foundations of this method were published by Matheron [63]. Nevertheless, it is Danie Gerhardus Krige who is considered the forerunner of the method.

The function interpolating by the kriging method has the form of the following equation [64]:

$$z_{KR}(x,y) = \sum_{i}^{n} w_i''(x,y) \cdot z_i \,, \tag{15}$$

where:
$z_{KR}(x,y)$ - height value of the interpolated point by the kriging method (m);
$w_i''(x,y)$ - weight value of the i-th point in the kriging method (-).

The kriging method consists of two stages. The first stage is to determine the spatial relationship between these data. In order to describe the spatial variability of the data, the kriging method usually uses half of the variogram, i.e. the so-called semivariogram, which is a graph showing the semivariance values as a function of distance. Therefore, before creating a semivariogram, semivariances need to be calculated for the interpolating points.

Semivariance is a measure that enables determination of the spatial autocorrelation, found in a particular set, i.e. the relationship between the values of a single feature that changes with the distance. This is half of the mean square of the difference between the values of the examined variable at two locations distant by the vector h [65]:

$$\gamma^*(h) = \frac{1}{2 \cdot N(h)} \sum_{i=1}^{N(h)} [z(x_i) - z(x_i + h)]^2 \,, \tag{16}$$

where:
$\gamma^*(h)$ - semivariance value calculated for distance h (m²);
$N(h)$ - number of paired data at a distance of h (-);
$z(x_i)$, $z(x_i+h)$ - height values at a particular location (m);
h - 3D Euclidean distance between the two interpolating points (m).

Once the semivariance has been calculated, the experimental semivariogram can be plotted (Figure 6) to represent the interpolating data on the semivariance graph as a function of distance.

A theoretical semivariogram must then be fitted to the experimental semivariogram (Figure 6) in such a manner that it best represents the empirical model. It should be noted that the best results of the interpolated values depend on the establishment of a correct semivariogram. Selected theoretical semivariogram models are described below and presented in Figure 7.

The spherical model has the form of [67]:

$$\gamma(h) = \begin{cases} C_0 + C_1 \cdot \left[\frac{3}{2} \cdot \left(\frac{h}{g} \right) - \frac{1}{2} \cdot \left(\frac{h}{g} \right)^3 \right] & h \le g \\ C_0 + C_1 & h > g \end{cases}, \tag{17}$$

Gaussian model [65]:

$$\gamma(h) = C_0 + C_1 \cdot \left[1 - e^{\left(\frac{-3 \cdot h^2}{g^2}\right)}\right], \quad (18)$$

while the linear model [65]:

$$\gamma(h) = C_0 + C_1 \cdot \left(\frac{h}{g}\right), \quad (19)$$

where:
$\gamma(h)$ - theoretical semivariogram model for distance h (m^2);

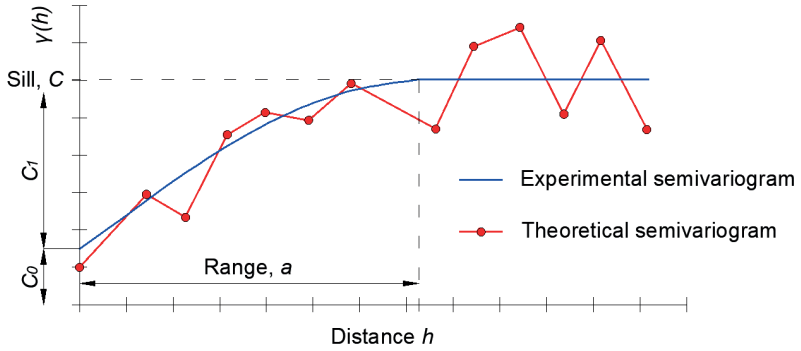

Figure 6 *A graph showing the experimental semivariogram along with the fitted theoretical semivariogram [66]*

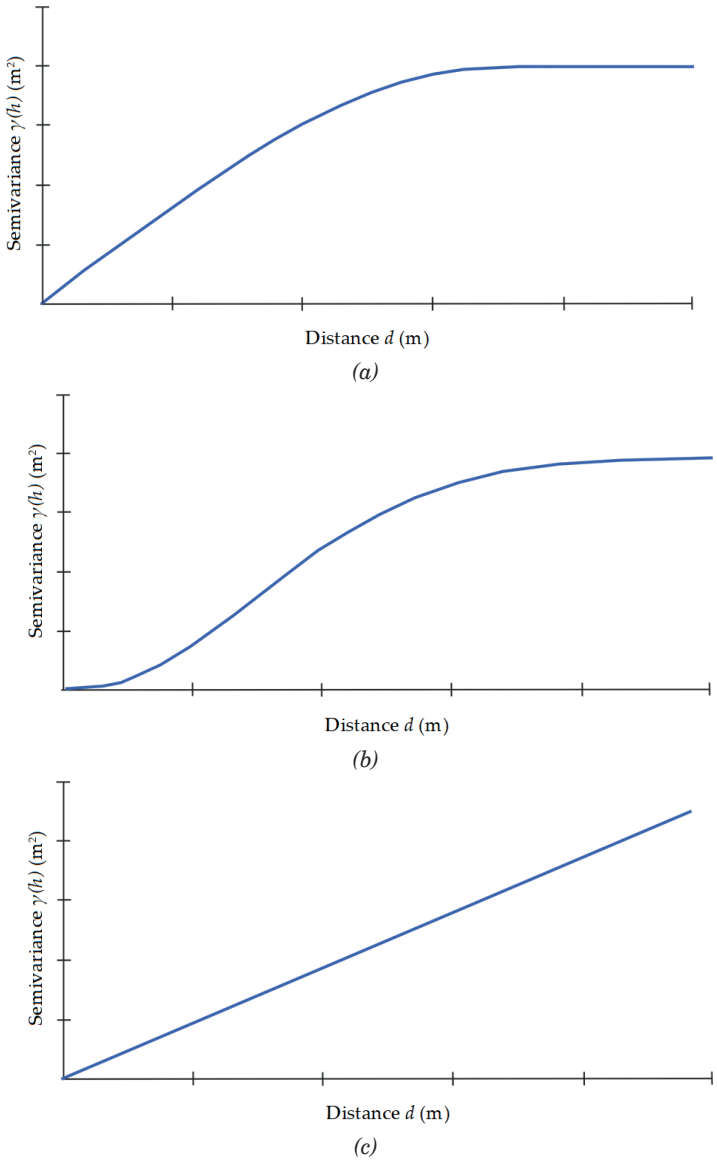

Figure 7 *Examples of the commonly used theoretical semivariogram models: spherical (**a**), Gaussian (**b**) and linear (**c**) [65]*

C_0, C_1 - nugget (unaccountable) and stochastic (accountable) variance (m²);
g - range of influence (m).

The second stage of the work concerns the calculation of the weights $w_i''(x,y)$. Based on the conducted analyses of the other interpolation methods, it must be concluded that the interpolation formula of the kriging method is similar to the IDW formula. Their similarity is due to the fact that the values assigned to the nearest point being interpolated are weighted. However, not only that the weights (referred to as kriging coefficients) are based on the distance between points, but on their spatial distribution, as well. These are determined from a set of equations resulting from the condition of minimizing error variance. This error (referred to as the kriging variance) is defined at measurement points as the difference between the interpolated value and the measurement value [68]:

$$\begin{bmatrix} \gamma(h_{11}) & \gamma(h_{12}) & \vdots & \gamma(h_{1n}) & 1 \\ \gamma(h_{21}) & \gamma(h_{22}) & \vdots & \gamma(h_{2n}) & 1 \\ \cdots & \cdots & \vdots & \cdots & \cdots \\ \gamma(h_{n1}) & \gamma(h_{n2}) & \vdots & \gamma(h_{nn}) & 1 \\ 1 & 1 & \vdots & 1 & 0 \end{bmatrix} \cdot \begin{bmatrix} w_1''(x,y) \\ w_2''(x,y) \\ \vdots \\ w_n''(x,y) \\ \lambda \end{bmatrix} = \begin{bmatrix} \gamma(h_1) \\ \gamma(h_2) \\ \vdots \\ \gamma(h_n) \\ 1 \end{bmatrix}, \quad (20)$$

where:
$\gamma(h_{ik})$ - semivariance between successive points i and k (m²);
$\gamma(h_i)$ - semivariance between the interpolated (unknown) point and the i-th point (m²);
λ - Lagrange multiplier (-).

Only after calculating the weights $w_i''(x,y)$ can one proceed to determine the values for the points being interpolated using Equation (15).

The kriging is among the most commonly used methods for interpolating geological parameters [69-71]. Geological measurements involve drilling the boreholes, as well as sampling soil and water at several locations. In most cases of interpolation methods, the generated model is inaccurate due to the small amount of data. Nevertheless, the kriging method is more effective for a smaller number of measurement points. This is primarily due to the possibility of the interpolation error in the model. However, it should be noted that in this method, not only that the results are determined by the number of measurement points but by the experimental semivariogram parameters and the mathematical model fitting, as well.

Moreover, this method is among the most accurate methods for creating a DTM [72-73]. This is evidenced by a study conducted by [74], who performed interpolation of the data derived from a SBES using different methods. The most accurate digital terrain model was obtained for the radial basis function and kriging methods.

2.5 Spline

Spline functions are an interpolation method used when the input data are diverse in terms of a particular feature. A DTM generated using spline functions is devoid of outliers. This results from the interpolation technique, which involves fitting the polynomial segment to the measurement data. The polynomials are created separately for each interval between the two successive points [75]. A fitted curve is continuous and smooth, i.e. it has a derivative at each point, which means that the slope of a curve on either side of the joining of two polynomials is the same.

Depending on the interpolation conditions and polynomial equations, there are various types of spline functions. However, the most well-known and common is the cubic spline interpolation [76-77]. A cubic spline is the function, which is a third-degree polynomial for each interval [78]:

$$f(x) = f_i(x) = A_i \cdot (x - x_1)^3 + B_i \cdot (x - x_i)^2 + \\ + C_i \cdot (x - x_i) + D_i \quad \text{for} \quad x_i \le x \le x_{i+1} \quad \text{and} \quad (21) \\ i \in \{0, \ldots, n-1\},$$

where:
$f(x)$ - cubic spline (-);
A_i, B_i, C_i, D_i - numerical coefficients of the i-th point (-).

A special case of the cubic spline is the so-called natural spline, which, additionally, satisfies the following condition:

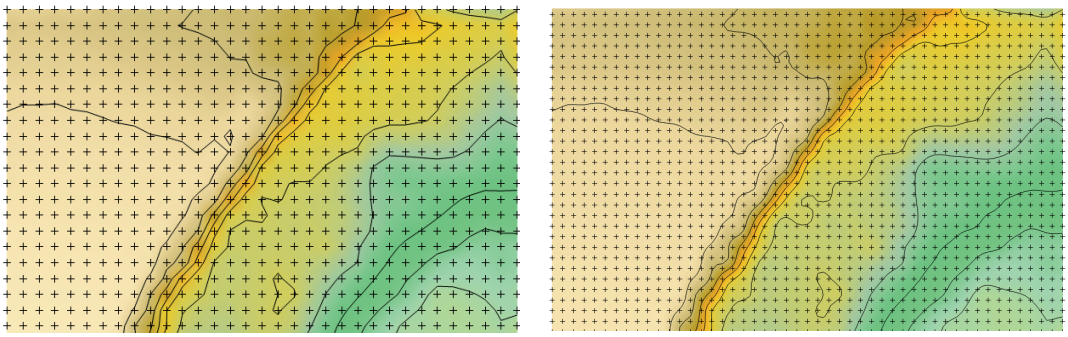

(a) *(b)*

Figure 8 *Isolines, the original surface (**a**) and its image after the spline smoothing (**b**)*

Table 1 *Summary of advantages and disadvantages of selected terrain modelling methods*

Terrain modelling method	Advantages	Disadvantages
IDW	Short computation time	It generates the so-called bull's-eye, i.e. concentric contours around measurement points
MSM	It receives similar results to those of the IDW but does not tend to generate the so-called bull's eye	Terrain deformations are formed
NNI	It receives good results for unevenly distributed data	It does not extrapolate the terrain relief
Kriging	It receives the best, non-affected linear estimations	Semivariogram modelling problem occurs
Spline	It forms a smooth surface	It is not suitable for points located close to each other and having different values

$$f''(x_0) = f''(x_n) = 0\,, \tag{22}$$

where:
$f''(x_0)$, $f''(x_n)$ - second derivatives of the cubic spline (-).

The literature and terrain modelling programs [79-80] mention the so-called smoothing spline. This method is based on the same definition of a spline function as that in Equation (21). The only modification is the values of the nodes. Each point (x_i, y_i) is replaced with a node (x_i, D_i).

Spline smoothing is a method applied when a map in the form of curves includes contours and surfaces refracted at different angles. The method application increases the model grid density, which results in the smoothing of the sharp refract of the isolines, thus minimizing the surface curvature. As a result, the interpolated surface is smooth (Figure 8).

The spline method was applied to interpolate the sea surface temperature in the southern part of the Indian Ocean [81]. Moreover, the model generated by the spline method was compared to the models interpolated by the IDW, NNI and kriging methods. Based on the conducted analyses, all of the methods were found to have similar RMSE values. North and Livingstone [82] compared the two methods that rely on the fitting of a polynomial to data. The two-point linear interpolation and cubic spline interpolation were applied to interpolate water column profiles in a lake. The results of the study showed that both methods are suitable for interpolating the incomplete input data.

3 Conclusions

In the coastal zone monitoring studies, optoelectronic and hydroacoustic methods are used [83]. However, these methods do not ensure the coverage with data of the entire coastal zone. Therefore, the terrain modelling methods are used [84]. Moreover, the land surface modelling in the coastal zone deserves particular attention, as the accurately mapped surface in this area is a part of coastal monitoring.

This study provides an overview of the most important terrain modelling methods. In the future, these methods will be applied to the real data derived from the coastal zone. Therefore, before proceeding to the data processing stage, it was decided to describe the selected interpolation methods, important in terms of the coastal zone modelling, using equations. Moreover, examples of the use of methods were provided in various areas, e.g. geology and meteorology. Table 1 presents advantages and disadvantages of selected terrain modelling methods.

It should be noted that the general characteristics of the methods provide no information on the fit between the terrain modelling method and the phenomenon [85-87]. This is due to the fact that each phenomenon being interpolated is characterized by different spatial distribution of measurement points, resulting from the data acquisition method applied. Therefore, the statistical analyses should be carried out for characteristic data in the selected area.

Acknowledgement

This research was funded by the National Centre for Research and Development in Poland, grant number LIDER/10/0030/L-11/19/NCBR/2020. Moreover, this research was funded from the statutory activities of Gdynia Maritime University, grant number WN/PI/2023/03.

Conflicts of interest

The authors declare that they have no known competing financial interests or personal relationships that could have appeared to influence the work reported in this paper.

References

[1] LUBCZONEK, J., KAZIMIERSKI, W., ZANIEWICZ, G., LACKA, M. Methodology for combining data acquired by unmanned surface and aerial vehicles to create digital bathymetric models in shallow and ultra-shallow waters. *Remote Sensing* [online]. 2021, **14**(1), 105. eISSN 2072-4292. Available from: https://doi.org/10.3390/rs14010105

[2] SPECHT, C., LEWICKA, O., SPECHT, M., DABROWSKI, P., BURDZIAKOWSKI, P. Methodology for carrying out measurements of the tombolo geomorphic landform using unmanned aerial and surface vehicles near Sopot Pier, Poland. *Journal of Marine Science and Engineering* [online]. 2020, **8**(6), 384. eISSN 2077-1312. Available from: https://doi.org/10.3390/jmse8060384

[3] STATECZNY, A., WLODARCZYK-SIELICKA, M., GRONSKA, D., MOTYL, W. Multibeam echosounder and LiDAR in process of 360-degree numerical map production for restricted waters with HydroDron. In: 2018 Baltic Geodetic Congress Geomatics 2018: proceedings. 2018.

[4] SPECHT, M., STATECZNY, A., SPECHT, C., WIDZGOWSKI, S., LEWICKA, O., WISNIEWSKA, M. Concept of an innovative autonomous unmanned system for bathymetric monitoring of shallow waterbodies (INNOBAT system). *Energies* [online]. 2021, **14**(17), 5370. eISSN 1996-1073. Available from: https://doi.org/10.3390/en14175370

[5] LI, J., HEAP, A. D. Spatial interpolation methods applied in the environmental sciences: a review. *Environmental Modelling and Software* [online]. 2014, **53**, p. 173-189. ISSN 1364-8152, eISSN 1873-6726. Available from: https://doi.org/10.1016/j.envsoft.2013.12.008

[6] SPECHT, C., SPECHT, M., DABROWSKI, P. Comparative analysis of active geodetic networks in Poland. In: 17th International Multidisciplinary Scientific GeoConference SGEM 2017: proceedings [online]. 2017. ISBN 978-619-7408-02-7, ISSN 1314-2704, p. 163-176. Available from: https://doi.org/10.5593/sgem2017/22/S09.021

[7] SPECHT, C., SZOT, T., DABROWSKI, P., SPECHT, M. Testing GNSS receiver accuracy in Samsung Galaxy series mobile phones at a sports stadium. *Measurement Science and Technology* [online]. 2020, **31**, 064006. ISSN 0957-0233, eISSN 1361-6501. Available from: https://doi.org/10.1088/1361-6501/ab75b2

[8] SPECHT, C., WEINTRIT, A., SPECHT, M. A history of maritime radio-navigation positioning systems used in Poland. *The Journal of Navigation* [online]. 2016, **69**(3), p. 468-480. ISSN 0373-4633, eISSN 1469-7785. Available from: https://doi.org/10.1017/S0373463315000879

[9] HELLWICH, O. Photogrammetric methods. In: *Encyclopedia of GIS* [online]. SHEKHAR, S., XIONG, H., ZHOU, X. (Eds.). Cham, Switzerland: Springer Cham, 2017. ISBN 978-3-319-17884-4, eISBN 978-3-319-17885-1, p. 1574-1580. Available from: https://doi.org/10.1007/978-3-319-17885-1

[10] BURDZIAKOWSKI, P., BOBKOWSKA, K. UAV photogrammetry under poor lighting conditions - accuracy considerations. *Sensors* [online]. 2021, **21**(10), 3531. eISSN 1424-8220. Available from: https://doi.org/10.3390/s21103531

[11] WANG, X., LIU, Y., LING, F., LIU, Y., FANG, F. Spatio-temporal change detection of Ningbo coastline using Landsat time-series images during 1976-2015. *ISPRS International Journal of Geo-Information* [online]. 2017, **6**(3), 68. eISSN 2220-9964. Available from: https://doi.org/10.3390/ijgi6030068

[12] NIKOLAKOPOULOS, K. G., LAMPROPOULOU, P., FAKIRIS, E., SARDELIANOS, D., PAPATHEODOROU, G. Synergistic use of UAV and USV data and petrographic analyses for the investigation of beach rock formations: a case study from Syros Island, Aegean Sea, Greece. *Minerals* [online]. 2018, **8**(11), 534. eISSN 2075-163X. Available from: https://doi.org/10.3390/min8110534

[13] SPECHT, M., SPECHT, C., MINDYKOWSKI, J., DABROWSKI, P., MASNICKI, R., MAKAR, A. Geospatial modeling of the tombolo phenomenon in Sopot using integrated geodetic and hydrographic measurement methods. *Remote Sensing* [online]. 2020, **12**(4), 737. eISSN 2072-4292. Available from: https://doi.org/10.3390/rs12040737

[14] DOUCETTE, P., AGOURIS, P., MUSAVI, M., STEFANIDIS, A. Road center line vectorization by self-organized mapping. *International Archives of Photogrammetry and Remote Sensing*. 2000, **XXXIII**(B3), p. 246-253. ISSN 1682-1750.

[15] WANG, C., HUANG, K., SHI, W. An accurate and efficient quaternion-based visualization approach to 2D/3D vector data for the mobile augmented reality map. *ISPRS International Journal of Geo-Information* [online]. 2022, **11**(7), 383. eISSN 2220-9964. Available from: https://doi.org/10.3390/ijgi11070383

[16] WILLIAMS, R., BRASINGTON, J., VERICAT, D., HICKS, M., LABROSSE, F., NEAL, M. Chapter twenty - monitoring braided river change using terrestrial laser scanning and optical bathymetric mapping. *Developments in Earth Surface Processes* [online]. 2011, **15**, p. 507-532. ISSN 0928-2025, eISSN 2213-588X. Available from: https://doi.org/10.1016/B978-0-444-53446-0.00020-3

[17] MARCHEL, L., NAUS, K., SPECHT, M. Optimisation of the position of navigational aids for the purposes of SLAM technology for accuracy of vessel positioning. *The Journal of Navigation* [online]. 2020, **73**(2), p. 282-295.

ISSN 0373-4633, eISSN 1469-7785. Available from: https://doi.org/10.1017/S0373463319000584
[18] SAYLAM, K., BROWN, R. A., HUPP, J. R. Assessment of depth and turbidity with airborne Lidar bathymetry and multiband satellite imagery in shallow water bodies of the Alaskan North Slope. *International Journal of Applied Earth Observation and Geoinformation* [online]. 2017, **58**, p. 191-200. ISSN 1569-8432, eISSN 1872-826X. Available from: https://doi.org/10.1016/j.jag.2017.02.012
[19] KETELAAR, V. B. H. (Gini). *Satellite radar interferometry* [online]. Dordrecht, Netherlands: Springer Dordrecht, 2009. ISBN 978-90-481-8125-4, eISBN 978-1-4020-9428-6. Available from: https://doi.org/10.1007/978-1-4020-9428-6
[20] SOLTANIEH, A., MACCIOTTA, R. Updated understanding of the Ripley landslide kinematics using satellite InSAR. *Geosciences* [online]. 2022, **12**(8), 298. eISSN 2076-3263. Available from: https://doi.org/10.3390/geosciences12080298
[21] VAN KREVELD, M. Digital elevation models and TIN algorithms. In: *Algorithmic foundations of geographic information systems* [online]. VAN KREVELD, M., NIEVERGELT, J., ROOS, T., WIDMAYER, P. (Eds.). Vol. 1340. Berlin, Heidelberg, Germany: Springer Berlin, Heidelberg, 1997. ISBN 978-3-540-63818-6, eISBN 978-3-540-69653-7, p. 37-78. Available from: https://doi.org/10.1007/3-540-63818-0_3
[22] MENG, Q., LIU, Z., BORDERS, B. E. Assessment of regression kriging for spatial interpolation - comparisons of seven GIS interpolation methods. *Cartography and Geographic Information Science* [online]. 2013, **40**(1), p. 28-39. ISSN 1523-040, eISSN 1545-0465. Available from: https://doi.org/10.1080/15230406.2013.762138
[23] GENCHI, S. A., VITALE, A. J., PERILLO, G. M. E., SEITZ, C., DELRIEUX, C. A. Mapping topobathymetry in a shallow tidal environment using low-cost technology. *Remote Sensing* [online]. 2020, **12**(9), 1394. eISSN 2072-4292. Available from: https://doi.org/10.3390/rs12091394
[24] PHAM, H. A new criterion for model selection. *Mathematics* [online]. 2019, **7**(12), 1215. eISSN 2227-7390. Available from: https://doi.org/10.3390/math7121215
[25] WILLMOTT, C. J., MATSUURA, K. Advantages of the mean absolute error (MAE) over the root mean square error (RMSE) in assessing average model performance. *Climate Research* [online]. 2005, **30**(1), p. 79-82. ISSN 0936-577X, eISSN 1616-1572. Available from: http://dx.doi.org/10.3354/cr030079
[26] CORTI, G., RANALLI, G., SOKOUTIS, D. Quantitative modelling of geological processes. *Tectonophysics* [online]. 2010, **484**(1-4), p. 1-3. ISSN 0040-1951, eISSN 1879-3266. Available from: https://doi.org/10.1016/j.tecto.2009.09.004
[27] TEOFILO, G., GIOIA, D., SPALLUTO, L. Integrated geomorphological and geospatial analysis for mapping fluvial landforms in Murge Basse Karst of Apulia (Southern Italy). *Geosciences* [online]. 2019, **9**(10), 418. eISSN 2076-3263. Available from: https://doi.org/10.3390/geosciences9100418
[28] LUBCZONEK, J., TROJANOWSKI, J., WLODARCZYK-SIELICKA, M. Application of threedimensional navigational information in electronic chart for inland shipping (in Polish). *Archives of Photogrammetry, Cartography and Remote Sensing*. 2012, **23**, p. 261-269. eISSN 2391-9477.
[29] LU, G. Y., WONG, D. W. An adaptive inverse-distance weighting spatial interpolation technique. *Computers and Geosciences* [online]. 2008, **34**(9), p. 1044-1055. ISSN 0098-3004, eISSN 1873-7803. Available from: https://doi.org/10.1016/j.cageo.2007.07.010
[30] LI, Z., WANG, K., MA, H., WU, Y. An adjusted inverse distance weighted spatial interpolation method. In: 3rd International Conference on Communications, Information Management and Network Security CIMNS 2018: proceedings [online]. 2018. ISSN 2352-538X. Available from: https://doi.org/10.2991/cimns-18.2018.29
[31] MAKAR, A., SPECHT, C., SPECHT, M., DABROWSKI, P., BURDZIAKOWSKI, P., LEWICKA, O. Seabed topography changes in the Sopot pier zone in 2010-2018 influenced by tombolo phenomenon. *Sensors* [online]. 2020, **20**(21), 6061. eISSN 1424-8220. Available from: https://doi.org/10.3390/s20216061
[32] BARTIER, P. M., KELLER, C. P. Multivariate interpolation to incorporate thematic surface data using inverse distance weighting (IDW). *Computers and Geosciences* [online]. 1996, **22**(7), p. 795-799. ISSN 0098-3004, eISSN 1873-7803. Available from: https://doi.org/10.1016/0098-3004(96)00021-0
[33] DAVIS, J. C. *Statistics and data analysis in geology*. 3. ed. Hoboken, NJ, USA: John Wiley & Sons, Inc., 2002. ISBN 978-0-471-17275-8.
[34] STATECZNY, A. *Comparative navigation methods* (in Polish). Gdansk, Poland: Gdansk Scientific Society, 2004. ISBN 83-87359-88-2.
[35] TOMCZAK, M. Spatial interpolation and its uncertainty using automated anisotropic inverse distance weighting (IDW) - cross-validation/jackknife approach. *Journal of Geographic Information and Decision Analysis*. 1998, **2**(2), p. 18-30. ISSN 1480-8943.
[36] MALEIKA, W. Inverse distance weighting method optimization in the process of digital terrain model creation based on data collected from a multibeam echosounder. *Applied Geomatics* [online]. 2020, **12**, p. 397-407. ISSN 1866-9298, eISSN 1866-928X. Available from: https://doi.org/10.1007/s12518-020-00307-6

[37] GOLDSZTEJN, P., SKRZYPEK, G. Applications of numeric interpolation methods to the geological surface mapping using irregularly spaced data (in Polish). *Polish Geological Review*. 2004, **52**, p. 233-236. ISSN 0033-2151.

[38] Surfer® user's guide - Golden software LLC [online] [accessed 2023-03-16]. Available from: https://downloads.goldensoftware.com/guides/Surfer20UserGuide.pdf

[39] PHOTHONG, T., DUMRONGCHAI, P., SIRIMONTREE, S., WITCHAYANGKOON, B. Spatial interpolation of unconfined compressive strength for soft Bangkok clay via random technique and modified inverse distance weight method. *International Transaction Journal of Engineering, Management, and Applied Sciences and Technologies* [online]. 2017, **8**(1), 13-22. ISSN 2228-9860, eISSN 1906-9642. Available from: http://TUENGR.COM/V08/013.pdf

[40] SHEPARD, D. A Two-dimensional interpolation for irregularly-spaced data. In: 23rd Association for Computing Machinery National Conference ACM 1968: proceedings [online]. 1968. p. 517-524. Available from: https://doi.org/10.1145/800186.810616

[41] FRANKE, R., NIELSON, G. Smooth interpolation of large sets of scattered data. *International Journal for Numerical Methods in Engineering* [online]. 1980, **15**(10), p. 1691-1704. eISSN 1097-0207. Available from: https://doi.org/10.1002/nme.1620151110

[42] RENKA, R. J. Multivariate interpolation of large sets of scattered data. *ACM Transactions on Mathematical Software* [online]. 1988, **14**(2), p. 139-148. ISSN 0098-3500, eISSN 1557-7295. Available from: https://doi.org/10.1145/45054.45055

[43] BASSO, K., DE AVILA ZINGANO, P. R., DAL SASSO FREITAS, C. M. Interpolation of scattered data: investigating alternatives for the modified Shepard method. In: 12th Brazilian Symposium on Computer Graphics and Image Processing: proceedings. 1999.

[44] MALVIC, T., IVSINOVIC, J., VELIC, J., SREMAC, J., BARUDZIJA, U. Application of the Modified Shepard's Method (MSM): a case study with the interpolation of neogene reservoir variables in Northern Croatia. *Stats* [online]. 2020, **3**(1), p. 68-83. eISSN 2571-905X. Available from: https://doi.org/10.3390/stats3010007

[45] JANKOVIC, V. Quadratic functions in several variables. *The Teaching of Mathematics* [online]. 2005, **VIII**(2), p. 53-60. ISSN 1451-4966, eISSN 2406-1077.

[46] ZEVENBERGEN, L. W., THORNE, C. R. Quantitative analysis of land surface topography. *Earth Surface Processes and Landforms* [online]. 1987, **12**(1), p. 47-56. eISSN 1096-9837. Available from: https://doi.org/10.1002/esp.3290120107

[47] SALKIND, N. *Encyclopedia of measurement and statistics* [online]. Vol. 2. Thousand Oaks, CA, USA: Sage Publications, 2007. ISBN 9781412916110, eISBN 9781412952644. Available from: https://doi.org/10.4135/9781412952644

[48] FRANKE, R. Scattered data interpolation: tests of some methods. *Mathematics of Computation* [online]. 1982, **38**(157), p. 181-200. ISSN 0025-5718. Available from: https://hdl.handle.net/10945/40152

[49] SIBSON, R. A Brief description of natural neighbor interpolation. In: *Interpreting multivariate data*. BARNETT, V. (Ed.). Hoboken, NJ, USA: John Wiley and Sons, Inc., 1981. ISBN 978-0471280392, p. 21-36.

[50] FARIN, G. Surfaces over Dirichlet tessellations. *Computer Aided Geometric Design* [online]. 1990, **7**(1-4), p. 281-292. ISSN 0167-8396, eISSN 1879-2332. Available from: https://doi.org/10.1016/0167-8396(90)90036-Q

[51] PIPER, B. Properties of local coordinates based on Dirichlet tessellations. In: *Geometric modelling*. FARIN, G., NOLTEMEIER, H., HAGEN, H., KNODEL, W. (Eds.). Vol. 8. Vienna, Austria: Springer Vienna, 1993. ISBN 3-211-83603-9, p. 227-239.

[52] CUETO, E., SUKUMAR, N., CALVO, B., MARTINEZ, M. A., CEGONINO, J., DOBLARE, M. Overview and recent advances in natural neighbour Galerkin methods. *Archives of Computational Methods in Engineering* [online]. 2003, **10**(4), p. 307-384. ISSN 1134-3060, eISSN 1886-1784. Available from: https://doi.org/10.1007/BF02736253

[53] SIBSON, R. A Vector identity for the Dirichlet tessellation. *Mathematical Proceedings of the Cambridge Philosophical Society* [online]. 1980, **87**(1), p. 151-155. ISSN 0305-0041, eISSN 1469-8064. Available from: https://doi.org/10.1017/S0305004100056589

[54] TAMASSIA, R. Introduction to Voronoi diagrams [online] [accessed 2023-03-16]. Available from: https://cs.brown.edu/courses/cs252/misc/resources/lectures/pdf/notes09.pdf

[55] LEDOUX, H., GOLD, C. An efficient natural neighbour interpolation algorithm for geoscientific modelling. In: *Developments in spatial data handling*. FISHER, P. F. (Ed.). Berlin, Heidelberg, Germany: Springer Berlin, Heidelberg, 2005. ISBN 978-3-540-22610-9, eISBN 978-3-540-26772-0, p. 97-108. Available from: https://doi.org/10.1007/3-540-26772-7_8

[56] VORONOI, G. A New A new applications of the continuous parameters in the theory of quadratic forms. First memoir. On some properties of the perfect positive quadratic forms (in English) *Journal for Pure and Applied Mathematics*. 1908, **134**, p. 97-178. ISSN 0075-4102, eISSN 1435-5345.

[57] THIESSEN, A. H. Precipitation averages for large areas. *Monthly Weather Review* [online]. 1911, **39**(7), p. 1082-1084. ISSN 0027-0644, elSSN 1520-0493. Available from: http://dx.doi.org/10.1175/1520-0493(1911)39<1082b:PAFLA>2.0.CO;2

[58] SCHUMANN, A. H. Thiessen polygon. In: *Hydrology and lakes. Encyclopedia of earth science*. HERSCHY, R. W., FAIRBRIDGE, R. W. (Eds.). Dordrecht, Netherlands: Springer Dordrecht, 1998. ISBN 9780412740602, p. 648-649.

[59] ANGELUCCI, G., MOLLAIOLI, F. Voronoi-like grid systems for tall buildings. *Frontiers in Built Environment* [online]. 2018, **4**, 78. eISSN 2297-3362. Available from: https://doi.org/10.3389/fbuil.2018.00078

[60] NONOGAKI, S., MASUMOTO, S., NEMOTO, T., NAKAZAWA, T. Voxel modeling of geotechnical characteristics in an urban area by natural neighbor interpolation using a large number of borehole logs. *Earth Science Informatics* [online]. 2021, **14**, p. 871-882. ISSN 1865-0473, eISSN 1865-0481. Available from: https://doi.org/10.1007/s12145-021-00600-x

[61] COLEMAN, J. B., YAO, X., JORDAN, T. R., MADDEN, M. Holes in the ocean: filling voids in bathymetric Lidar data. *Computers and Geosciences* [online]. 2011, **37**(4), p. 474-484. ISSN 0098-3004, eISSN 1873-7803. Available from: https://doi.org/10.1016/j.cageo.2010.11.008

[62] KLEIJNEN, J. P. C. Kriging metamodeling in simulation: a review. *European Journal of Operational Research* [online]. 2009, **192**(3), p. 707-716. ISSN 0377-2217, eISSN 0377-2217. Available from: https://doi.org/10.1016/j.ejor.2007.10.013

[63] MATHERON, G. Principles of geostatistics. *Economic Geology* [online]. 1963, **58**(8), p. 1246-1266. ISSN 0361-0128, eISSN 1554-0774. Available from: http://dx.doi.org/10.2113/gsecongeo.58.8.1246

[64] FANCHI, J. R. Chapter 2 - Geological modeling. In: *Principles of applied reservoir simulation*. FANCHI, J. R. (Ed.). 4. ed. Houston, TX, USA: Gulf Professional Publishing, 2018. ISBN 9780128155639, eISBN 9780128155646, p. 9-33.

[65] MERT, B. A., DAG, A. A Computer program for practical semivariogram modeling and ordinary kriging: a case study of porosity distribution in an oil field. *Open Geosciences* [online]. 2017, **9**(1), p. 663-674. ISSN 2391-5447. Available from: https://doi.org/10.1515/geo-2017-0050

[66] WONG, A. H., KWON, T. J. Advances in regression kriging-based methods for estimating statewide winter weather collisions: an empirical investigation. *Future Transportation* [online]. 2021, **1**(3), p. 570-589. eISSN 2673-7590. Available from: https://doi.org/10.3390/futuretransp1030030

[67] MONTES, F., HERNANDEZ, M. J., CANELLAS, I. A Geostatistical approach to cork production sampling estimation in Quercus Suber Forests. *Canadian Journal of Forest Research*. 2013, **35**(12), p. 2787-2796. ISSN 0045-5067.

[68] JOURNEL, A. G., HUIJBREGTS, CH. J. *Mining geostatistics*. London, UK: Academic Press, 1978. ISBN 0123910501.

[69] CHE, D., JIA, Q. Three-dimensional geological modeling of coal seams using weighted kriging method and multi-source data. *IEEE Access* [online]. 2019, **7**, p. 118037-118045. eISSN 2169-3536. Available from: https://doi.org/10.1109/ACCESS.2019.2936811

[70] DAI, H., REN, L., WANG, M., XUE, H. Water distribution extracted from mining subsidence area using kriging interpolation algorithm. *Transactions of Nonferrous Metals Society of China* [online]. 2011, **21**(s3), s723-s726. ISSN 1003-6326, eISSN 2210-3384. Available from: https://doi.org/10.1016/S1003-6326(12)61669-0

[71] MALVIC, T., IVSINOVIC, J., VELIC, J., RAJIC, R. Kriging with a small number of data points supported by jack-knifing, a case study in the Sava Depression (Northern Croatia). *Geosciences* [online]. 2019, **9**(1), 36. eISSN 2076-3263. Available from: https://doi.org/10.3390/geosciences9010036

[72] VAN BEERS, W. C. M., KLEIJNEN, J. P. C. Kriging for interpolation in random simulation. *Journal of the Operational Research Society* [online]. 2003, **54**(3), p. 255-262. ISSN 0160-5682, eISSN 1476-9360. Available from: https://doi.org/10.1057/palgrave.jors.2601492

[73] WOJCIECH, M. Kriging method optimization for the process of DTM creation based on huge data sets obtained from MBESs. *Geosciences* [online]. 2018, **8**(12), 433. eISSN 2076-3263. Available from: https://doi.org/10.3390/geosciences8120433

[74] PARENTE, C., VALLARIO, A. Interpolation of single beam echo sounder data for 3D bathymetric model. *International Journal of Advanced Computer Science and Applications (IJACSA)* [online]. 2019, **10**(10), p. 6-13. ISSN 2158-107X, eISSN 2156-5570. Available from: https://doi.org/10.14569/IJACSA.2019.0101002

[75] LAM, N. S.-N. Spatial interpolation methods: a review. *The American Cartographer* [online]. 1983, **10**(2), p. 129-150. ISSN 1523-0406, eISSN 1545-0465. Available from: https://doi.org/10.1559/152304083783914958

[76] CHAPRA, S. C., CANALE, R. P. *Numerical methods for engineers*. 6. ed. New York, NY, USA: McGraw Hill, 2009. ISBN 978-0-07-340106-5.

[77] BURDEN, R. L., FAIRES, J. D. *Numerical analysis*. 9. ed. Boston, MA, USA: Brooks/Cole Publishing Company, 2010. ISBN 978-0-538-73351-9.

[78] DIAZ-ARAUJO, M., MEDINA, A., CISNEROS-MAGANA, R., RAMIREZ, A. Periodic steady state assessment of microgrids with photovoltaic generation using limit cycle extrapolation and cubic splines. *Energies* [online]. 2018, **11**(8), 2096. eISSN 1996-1073. Available from: https://doi.org/10.3390/en11082096

[79] Surfer help - Grid spline smooth [online] [accessed 2023-03-16]. Available from: https://surferhelp.goldensoftware.com/gridmenu/idm_splinesmooth.htm

[80] WANG, Y. *Smoothing splines: methods and applications* [online]. 1. ed. London, UK: Chapman and Hall/CRC, 2011. eISBN 9780429146923. Available from: https://doi.org/10.1201/b10954

[81] KUSUMA, D., MURDIMANTO, A., SUKRESNO, B., JATISWORO, D. Comparison of interpolation methods for sea surface temperature data. *JFMR (Journal of Fisheries and Marine Research)* [online]. 2018, **2**(2), p. 103-115. eISSN 2581-0294. Available from: https://doi.org/10.21776/ub.jfmr.2018.002.02.7

[82] NORTH, R. P., LIVINGSTONE, D. M. Comparison of linear and cubic spline methods of interpolating lake water column profiles: interpolation of lake profiles. *Limnology and Oceanography: Methods* [online]. 2013, **11**(4), p. 213-224. eISSN 1541-5856. Available from: https://doi.org/10.4319/lom.2013.11.213

[83] LEWICKA, O., SPECHT, M., STATECZNY, A., SPECHT, C., BRCIC, D., JUGOVIC, A., WIDZGOWSKI, S., WISNIEWSKA, M. Analysis of GNSS, hydroacoustic and optoelectronic data integration methods used in hydrography. *Sensors* [online]. 2021, **21**(23), 7831. eISSN 1424-8220. Available from: https://doi.org/10.3390/s21237831

[84] KARAKI, A. A., BIBULI, M., CACCIA, M., FERRANDO, I., GAGLIOLO, S., ODETTI, A., SGUERSO, D. Multi-platforms and multi-sensors integrated survey for the submerged and emerged areas. *Journal of Marine Science and Engineering* [online]. 2022, **10**(6), 753. eISSN 2077-1312. Available from: https://doi.org/10.3390/jmse10060753

[85] STATECZNY, A. The neural method of sea bottom shape modelling for the spatial maritime information system. In: *Maritime engineering and ports II*. BREBBIA, C.A., OLIVELLA, J. (Eds.). Vol. 51. Southampton, UK: WIT Press, 2000. ISBN 1-85312-829-5, p. 251-259.

[86] WLODARCZYK-SIELICKA, M., STATECZNY, A. Fragmentation of hydrographic big data into subsets during reduction process. In: Baltic Geodetic Congress 2017 BGC 2017: proceedings [online]. IEEE. 2017. ISBN 978-1-5090-6041-2, eISBN 978-1-5090-6040-5. Available from: https://doi.org/10.1109/BGC.Geomatics.2017.67

[87] WLODARCZYK-SIELICKA, M., STATECZNY, A., LUBCZONEK, J. The reduction method of bathymetric datasets that preserves true geodata. *Remote Sensing* [online]. 2019, **11**(13), 1610. eISSN 2072-4292. Available from: https://doi.org/10.3390/rs11131610


1953
70
2023
ŽILINSKÁ UNIVERZITA V ŽILINE
BioTechUSA
SOM VEDEC
PYTAJTE SA MA
NOC
drobtak
Stavebná fakulta
BA BB
E 499062